NANO LETTERS

Letter

pubs.acs.org/NanoLett

High-Performance *a*-Si/*c*-Si Heterojunction Photoelectrodes for Photoelectrochemical Oxygen and Hydrogen Evolution

Hsin-Ping Wang,[†,‡,▽] Ke Sun,[‡] Sun Young Noh,[∥] Alireza Kargar,[‡] Meng-Lin Tsai,[†] Ming-Yi Huang,[§] Deli Wang,*[,‡,∥,⊥] and Jr-Hau He*[,‡,†]

[†]Computer, Electrical and Mathematical Sciences and Engineering (CEMSE) Division, King Abdullah University of Science & Technology (KAUST), Thuwal 23955-6900, Kingdom of Saudi Arabia

[‡]Department of Electrical and Computer Engineering, University of California−San Diego, 9500 Gilman Drive, La Jolla, California 92093, United States of America

[§]Advanced Technology Department, AU Optronic Corporation, Taichung, Taiwan, Republic of China

[∥]Materials Science and Engineering Program, University of California−San Diego, 9500 Gilman Drive, La Jolla, California 92093, United States of America

[⊥]Qualcomm Institute, University of California−San Diego, 9500 Gilman Drive, La Jolla, California 92093, United States of America

[▽]Institute of Photonics and Optoelectronics and Department of Electrical Engineering, National Taiwan University, Taipei 10617, Taiwan

Supporting Information

ABSTRACT: Amorphous Si (*a*-Si)/crystalline Si (c-Si) heterojunction (SiHJ) can serve as highly efficient and robust photoelectrodes for solar fuel generation. Low carrier recombination in the photoelectrodes leads to high photocurrents and photovoltages. The SiHJ was designed and fabricated into both photoanode and photocathode with high oxygen and hydrogen evolution efficiency, respectively, by simply coating of a thin layer of catalytic materials. The SiHJ photoanode with sol−gel NiO_x as the catalyst shows a current density of 21.48 mA/cm^2 at the equilibrium water oxidation potential. The SiHJ photocathode with 2 nm sputter-coated Pt catalyst displays excellent hydrogen evolution performance with an onset potential of 0.640 V and a solar to hydrogen conversion efficiency of 13.26%, which is the highest ever reported for Si-based photocathodes.

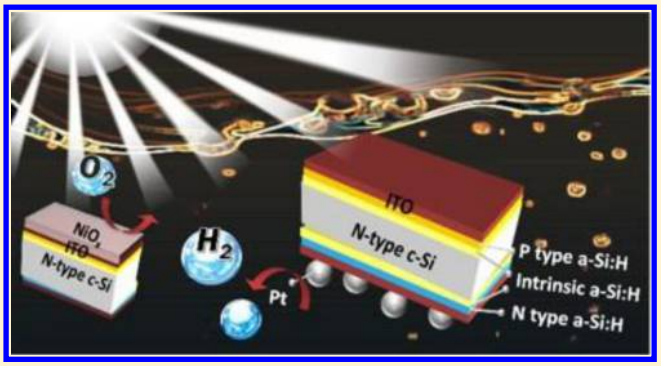

KEYWORDS: *Si heterojunction photoelectrodes, oxygen evolution, hydrogen evolution, solar to oxygen conversion efficiency, solar to hydrogen conversion efficiency*

Because of the steep increase in global energy demand and the serious effects of climate change, exploiting consecutive, eco-friendly, and cost-effective energy resources has become the top priority of research and development. The sun delivers energy to the earth in less than 2 h sufficient to provide our annual energy consumption. Solar energy is such a large source of energy that it has attracted researchers to develop the technology needed to convert intermittently available solar energy into stable and storable fuels, for example, by splitting water into hydrogen and oxygen by a combination of photovoltaic (PV) and electrolyzer technology. In order to achieve efficient self-biasing photoelectrochemical (PEC) systems, photoelectrodes are required that can supply a thermodynamic potential of 1.23 V for spontaneous overall water splitting (considering all losses, the band gap required for practical devices is about 1.6−2.4 eV)[1] while at the same time to absorb wide solar spectrum. Single materials with suitable band gaps for splitting water are limited by insufficient absorption of the visible and infrared spectra. Also, for those materials with the appropriate band gap, the conduction band or valence band of the photoelectrodes should properly align for water reduction or oxidation. Additionally, it is important to have robust PEC materials that are not prone to decomposition or corrosion. There is currently no single material that can be used for efficient solar water splitting. To overcome this problem, it is necessary to combine two or multiple materials with different band gaps to absorb a larger portion of the solar spectrum while simultaneously to provide the necessary overall photovoltage to split water.[2]

Photocathode + photoanode configurations or tandem absorber + electrocatalyst configurations have the potential to

Received: October 29, 2014
Revised: February 4, 2015

DOI: 10.1021/nl5041463
Nano Lett. XXXX, XXX, XXX−XXX

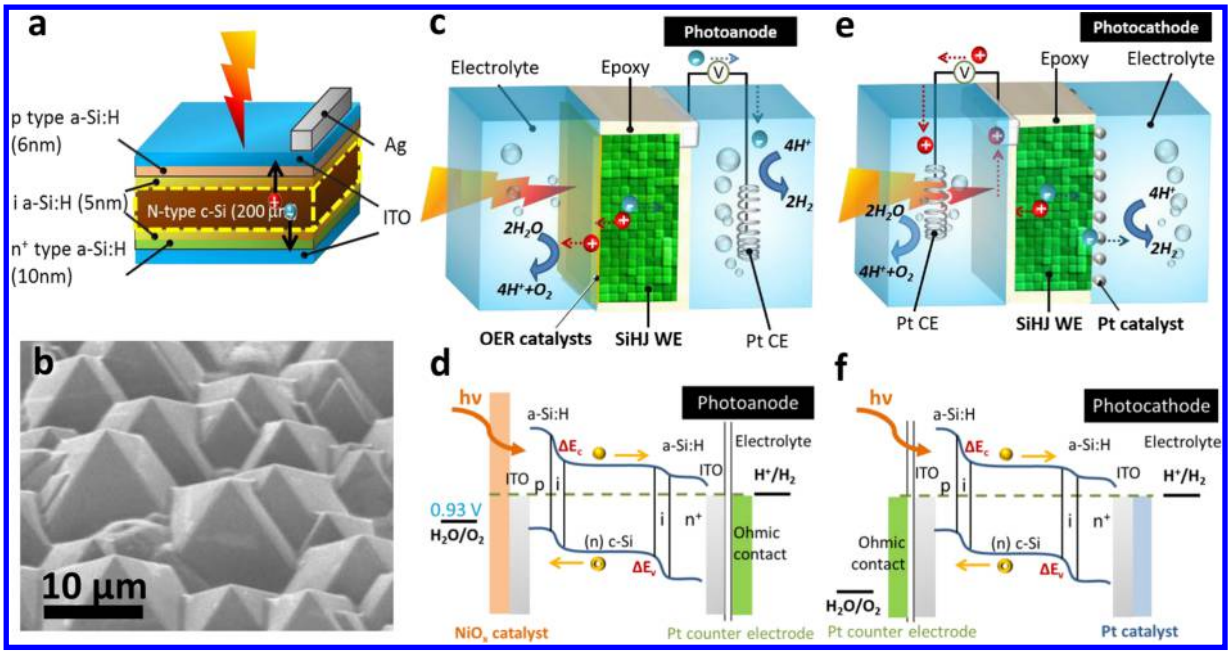

Figure 1. (a) Schematic of the SiHJ solar cell and (b) SEM image of the micropyramidal surfaces of the SiHJ photoelectrode; (c) schematic and (d) energy band diagrams of the SiHJ photoanode; (e) schematic and (f) the energy band diagrams of the SiHJ photocathode.

be used in self-biasing integrated PEC water-splitting systems. It has been reported that two-photoabsorber configurations with a top-junction band gap of 1.65−1.8 eV and bottom-junction band gap of 0.95−1.15 eV could theoretically reach a solar-to-hydrogen (STH) production efficiency (η_{STH}) higher than 25%.[2] Clearly, Si is an attractive candidate for constructing a multiple-photoabsorber configuration because of its suitable band gap (band gap of 1.1 eV), abundance in the earth's crust, and the vast amount of existing knowledge related to its use in the electronics and PV industries.[3,4] However, the inherent redox instability and poor PEC performance observed to date place serious limitations on the application of Si-based photoelectrodes. Recently, researchers have made considerable progresses on developing protective layers for Si-based photoelectrodes.[5−11] Chen et al. reported on a Si photoanode that can operate for at least 8 h fabricated using ultrathin ALD-deposited TiO_2 protective layers.[5] Kenney et al. showed that Ni/NiO_x could serve as a good conductive protective layer for photoanodes, which could still work after 80 h of operation in mild pH conditions.[7] Shu et al. demonstrated 100 h long stability in 1 M KOH using a thick "leaky" TiO_2-protected Si photoanodes with Ni metal island arrays.[10] TiO_2 has also been widely used as a good protective layer for photocathodes. Lin et al. used TiO_2 as a protective layer for amorphous Si (*a*-Si) photocathodes, achieving stability after 12 h of operation.[11] Seger et al. used Ti/TiO_2 layers to protect Si photocathodes that could keep working for over 30 days of operation.[8]

However, there has been no significant progress in terms of PEC performance. To date, the highest recorded solar-to-hydrogen conversion efficiency (SHCE) of a Si-based photocathode was 9.6% in 2011.[12] There is still room for improvement in both the photocurrent and photovoltage to achieve a higher PEC performance. The low photocurrent is mainly caused by the deposition of light-blocking catalysts on the light-illuminated side and the insufficient light trapping ability of planar Si. Many groups have proposed enhancing light absorption by using wired structures to enhance the light-trapping effect. However, without good surface passivation, there is no significant improvement in the photocurrent density, and the photovoltage might decrease due to the high surface defects. The optical losses caused by light-blocking catalysts can be solved by separating the PV effect from the water redox reactions.[13,14] In this way, the catalysts and the PV cells can be adjusted independently. In order to achieve this design, the low recombination of photoelectrodes is critical to avoid the photogenerated carrier recombination loss during the carrier transport through the whole devices to participate in water redox reaction.

In the past few decades, it has been shown in many studies that the liquid junction caused by band bending between the Si/electrolyte interface produces low photovoltage and is not sufficient to provide adequate electron−hole separation without proper surface modification.[8] More recent techniques, like buried p−n junctions, have attracted considerable attention due to their higher photovoltage production than liquid junctions and their electrolyte independence.[12] However, the photovoltage of buried junction crystalline Si (c-Si) photoelectrodes is still less than half of the value required for overall water splitting (1.23 V).[15] Success has been limited due to the poor surface passivation of Si. Therefore, good surface passivation is the best route to simultaneously improve both the photocurrent and photovoltage of Si photoelectrodes.

Si heterojunction (SiHJ) cell consisting of ultrathin a-Si layers on c-Si is a promising approach to meet this goal. The thin *a*-Si layers serve not only as emitter layers but also as good passivation layers. Here, we report on the use of the surface textured SiHJ PEC cells as efficient and robust photoelectrodes. Specifically, we demonstrate the functioning of SiHJ PEC cells coated with sol−gel NiO_x and metal thin layers serving as photoanodes (Figure 1c,d) and photocathodes (Figure 1e,f) for solar-to-oxygen and -hydrogen conversion, respectively. A $V_{OS}'-E^{0\prime}$ of up to 640 mV makes the SiHJ a good candidate for Si-based photoelectrodes, where V_{OS}' is the onset potential measured at a water reduction current density of 1 mA/cm^2, and $E^{0\prime}$ is the equilibrium water reduction potential.

DOI: 10.1021/nl5041463
Nano Lett. XXXX, XXX, XXX−XXX

SiHJ Photoelectrodes. So far, because of the small photovoltage produced by Si working electrodes (WEs), the use of Si as the part of the photocathode + photoanode or tandem absorber + electrocatalyst PEC configuration has been greatly limited.[2,12,16] The production of a large photovoltage is urgently desired. The high open-circuit voltage (V_{OC}) is the most distinguishing feature of SiHJ cells, made possible because the thin hydrogenated amorphous Si (*a*-Si:H) layers serve as good passivation layers on both the front and back contacts. The density of interface defects and carrier recombination can be reduced by surface chemical passivation and field-effect passivation.[17] Details of the SiHJ solar cell configuration are shown in Figure 1a. In our SiHJ cell, the ultrathin intrinsic *a*-Si:H on both sides of the n-type c-Si significantly passivates dangling bonds on the c-Si surface, leading to low densities of surface states and thus high quality junctions.[18,19] In addition, because of the large band gap of *a*-Si, the large band offset of the valence band and the conduction band (ΔE_c and ΔE_v) between *a*-Si:H/c-Si interface forms a barrier inhibiting the carrier recombination (Figure 1d,f), which leads to additional field-effect passivation. All the properties derived from the *a*-Si passivation layer suppress the dark saturation current, resulting in an outstanding photovoltage.[19−21] The passivation effect was investigated through the quasi-steady-state photoconductance measurement of minority carrier lifetime (Figure S1 in Supporting Information). There was a significant increase in the carrier lifetime from 47.29 to 386.22 μs at a minority carrier density of 10^{15} cm^{-3} after the intrinsic *a*-Si:H passivation. A high V_{OC} of 670 mV can be obtained (Table 3). Because of the effective passivation of the *a*-Si:H layers, a record high efficiency among all kinds of Si-based solid-state cells of commercial size (143.7 cm^2) of 25.6% was achieved by the Panasonic Corporation in 2014.[22]

Micropyramidal structures fabricated using KOH anisotropic etching are employed on both sides of the SiHJ PEC cells to enhance the light trapping and the surface reactive sites (Figure 1b).[23] The Tafel slope of substrates with pyramidal surfaces (19.4 mV/decade) is 1.25 times lower than that of substrates with planar surfaces (25.6 mV/decade) (Figure S2 in Supporting Information). The enhanced catalytic performance is attributed to enhanced semiconductor/electrolyte interfaces, which slow the hydrogen generation kinetics at the electrode and are able to load more amount of catalysts.[24] Compared to the micropyramidal structure, the high density of defect states caused by the large surface area of the nanostructures will typically result in a high recombination rate. The low carrier lifetime strongly affects the dark saturation current and thus the V_{OC}.[25] Despite the excellent light-harvesting characteristics and high number of reactive sites in the nanostructures, poor performance is unavoidable unless the surface can be successfully passivated.[21] Our SiHJ cells with the micropyramidal structures exhibited a high short-circuit current density (J_{SC}) of 35.41 mA/cm^2, a V_{OC} of 670 mV, and a conversion efficiency of 14.93%. The high V_{OC} demonstrates that the micropyramidal structures have been well passivated by the *a*-Si:H layer deposited by the plasma-enhanced chemical vapor deposition process.

SiHJ PEC cells can be designed to function as photoanodes or photocathodes by simply switching the polarity. Details of the process for fabrication of photoanodes or photocathodes with different catalysts are indicated in the Supporting Information. Figure 1c,e shows a schematic of the photoanode/photocathode operation setup. The three-electrode 1-compartment setup used for half-cell measurement consisted of a Pt counter electrode (CE), a Hg/HgO reference electrode (RE) in 1 M NaOH or Ag/AgCl RE in 1 M H_2SO_4, and the SiHJ cell as a WE. For the use of SiHJ as a photoanode, highly transparent oxygen-evolution-reaction (OER) catalysts were deposited on the anode side of the SHJs (Figure 1c). Once the photogenerated carriers are excited and separated, the photogenerated holes (lower mobility and short diffusion length in n-type wafer than electrons) immediately transport across the ITO to the OER catalyst where they participate in the water oxidation reaction. Photogenerated electrons (higher mobility and long diffusion length in *n*-type wafer than holes) transport throughout the wafer and are collected by the ITO cathode to the Pt CE, as shown in Figure 1c. For the SiHJ cell to serve as a photocathode, Pt, one of the well-known metal catalysts that promotes efficient proton reduction, is deposited on the ITO cathode of the SiHJ cell (Figure 1e). Figure S3 in Supporting Information shows the photographs of a SiHJ photoanode and a SiHJ photocathode. The difference in the design between the photoanode and the photocathode depends on the diffusion length of the minority carriers of the WE and the transmittance of the catalysts. ITO electrodes are applied to efficiently extract photogenerated carriers with minimal loss via the Ohmic contact between the Si/ITO interface (Figure 1d,f) while at the same time isolating Si from coming into contact with the electrolyte and metal catalysts.

SiHJ Photoanodes. Ni-based OER electrocatalysts have been widely studied as the active and stable earth-abundant materials for water oxidation.[7,26−29] In this study, four kinds of Ni-based OER catalysts were deposited on the SiHJ photoanode and then systematically studied, including metallic Ni, NiO_x, and $NiRuO_x$ using the sputter deposition, and NiO_x using the sol−gel spin coating method. Figure 2a shows a cyclic voltammetric (CV) measurements of SiHJ photoanodes with different thicknesses of metallic Ni in a 1 M NaOH electrolyte. Although the highest saturation current density (J_{SA}) is obtained from the SiHJ photoanode coated with 2 nm Ni catalysts, the low slope after onset caused by the insufficient catalytic activity restricts the J_{H_2O/O_2}, which indicates the current density at the equilibrium water oxidation potential in the 1 M NaOH solution. Increasing the thickness of the Ni coating gradually increases the slope after onset, but at the same time blocks the light absorption (see Figure S4 in Supporting Information). The local maximum conversion efficiency was achieved with 5 nm Ni due to the balance between the transmittance and catalytic activity. The elemental composition of 5 nm Ni before and after catalyst activation is evidenced by the X-ray photoelectron spectra (XPS, Figure S5 in Supporting Information). After catalyst activation, the increase in Ni(III) and Ni(II) was observed by XPS because during the oxygen evolution reaction, Ni is converted to $Ni(OH)_2$ and then to NiOOH. Although, the peak of metallic Ni significantly decreases after activation but is still observed by XPS, suggesting that the films were partially oxidized.

After optimizing the conditions for each Ni-based OER catalyst (Figure S6 and Table S1 in Supporting Information and refs 27−29), the best condition of Ni-based OER catalyst was coated onto SiHJ PEC cells. Figure 2b shows the CV measurements of a representative SiHJ photoanode with four different Ni-based OER catalysts under an simulated air mass of 1.5 global (AM 1.5G) illumination after 75 cycles of catalyst activation in a 1 M NaOH electrolyte at a scan rate of 100 mV/

DOI: 10.1021/nl5041463
Nano Lett. XXXX, XXX, XXX−XXX

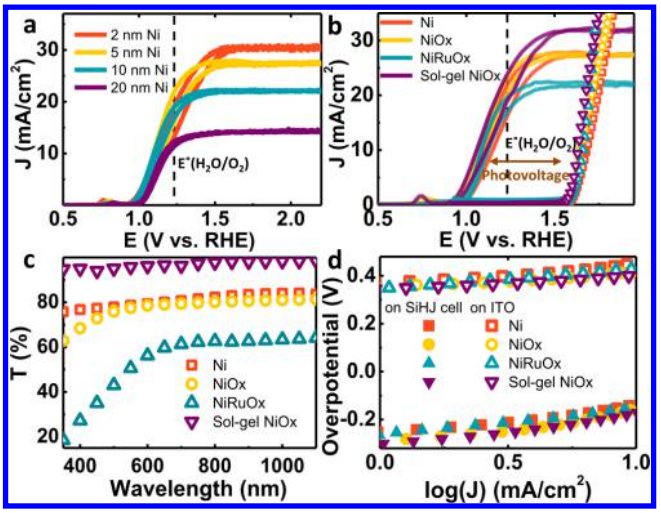

Figure 2. (a) $J-E$ behaviors of the SiHJ photoanodes with different thicknesses of Ni used as OER catalysts in a 1 M NaOH electrolyte under simulated AM 1.5G illumination. (b) $J-E$ behaviors of different Ni-based materials coated onto ITO films in a 1 M NaOH electrolyte in the dark (plotted symbols) and the SiHJ photoanodes with different Ni-based OER catalysts under simulated AM 1.5G illumination (solid line). (c) Total transmittance spectra of different Ni-based OER catalysts over the wavelength regions of 350−1100 nm. (d) Tafel plots of different Ni-based OER catalysts coated onto ITO films in a 1 M NaOH electrolyte in the dark (open symbol) and the SiHJ photoanodes with different Ni-based OER catalysts under simulated AM 1.5G illumination (solid symbols).

s (solid line). In order to isolate the catalytic effect from the PV effect in the SiHJ photoanode, electrochemical characterization of four Ni-based OER catalysts coated onto ITO films is carried out, as plotted in Figure 2b (plotted symbols). When applying the potential through the ITO film with OER catalysts in the dark (Figure 2b, plotted symbols), a large bias of 1.633 V vs RHE must be applied to reach the current density of 10 mA/cm^2, implying an overpotential of 0.403 V (for sol−gel NiO_x), which agrees with the required overpotential of NiO_x catalysts for oxygen evolution.[30] After illumination, all of the current onsets shifted to more negative potentials than the oxygen evolution potential (vertical dotted line). A much lower potential of 1.06 V vs RHE (for sol−gel NiO_x) is needed to attain a current density of 10 mA/cm^2. The reduction of the required applied potential stems from the high photovoltage generated by the SiHJ photoanode.

Solar-to-Oxygen Conversion Efficiency (SOCE). The SOCE was calculated as follows:

$$\mathrm{SOCE} = \frac{|V_{OS} - E^0|J_{H_2O/O_2}FF}{I_{ph}} \quad (1)$$

where V_{OS} is the onset potential measured at a water oxidation current density of 1 mA/cm^2; E^0 is the equilibrium water oxidation potential in the 1 M NaOH electrolyte, which is 1.23 V vs RHE; FF is the fill factor measured at a water oxidation current density of 1 mA/cm^2; and I_{ph} is the incident optical power density. The calculated SOCE, representing the upper limit of the conversion efficiency under the applied bias for a half cell, is summarized in Table 1.[29,31] The SiHJ photoanode with the sol−gel NiO_x catalyst reaches the highest efficiency, 1.5%, due to high transmittance and catalytic activity of the sol−gel NiO_x catalyst. The tendency of transmittance for each

Table 1. Characteristics of the SiHJ Photoanodes with Different Ni-Based Materials as OER Catalysts in the 1 M NaOH Electrolyte under AM 1.5G Illumination; the Onset Potential Measured at 1 mA/cm^2

	J_{H_2O/O_2} (mA/cm^2)	$V_{OS} - E^0$ (V)	FF (%)	SOCE (%)
Ni	18.93	0.241	24.5	1.12
NiO_x	21.64	0.272	24.3	1.43
$NiRuO_x$	18.15	0.241	29.6	1.29
sol−gel NiO_x	21.48	0.291	24.0	1.50

Ni-based OER catalyst (Figure 2c) is consistent with that of J_{SA} as seen in Figure 2b. For the sol−gel NiO_x sample, the average transmittance reaches as high as 96.79% from 350 to 1100 nm, and the J_{H_2O/O_2} exceeds 21 mA/cm^2. At greater applied potentials, the photocurrent density became saturated at 32.67 mA/cm^2. Such a high current density is made possible by the significant light trapping and low photocarrier recombination loss of the SiHJ PEC cells, combined with the high transmittance and good catalytic performance of the sol−gel NiO_x catalyst.

Tafel Slopes and Overpotentials. The catalytic performance was investigated by a Tafel plot. Figure 2d shows the corresponding Tafel plots for SiHJ photoanodes under simulated AM 1.5G illumination (solid symbols), and the ITO film with the OER catalyst in the dark (open symbols). Quantitative information for the Tafel slopes and overpotentials is summarized in Table 2. The Tafel slopes and overpotentials

Table 2. Summary of Tafel Slopes and Overpotentials for SiHJ Photoanodes from Different Ni-Based Materials Used as OER Catalysts in the 1 M NaOH Electrolyte under simulated AM 1.5G Illumination; the Overpotential Was Measured at 1 mA/cm^2

	Tafel slope (mV/decade)		overpotential (V)	
	dark (on ITO)	light (on SiHJ WE)	dark (on ITO)	light (on SiHJ WE)
Ni	52.0	62.0	0.370	−0.241
NiO_x	30.0	58.6	0.358	−0.272
$NiRuO_x$	38.9	90.0	0.345	−0.241
sol−gel NiO_x	41.4	51.3	0.346	−0.291

were measured in the dark to represent the catalytic performance. The two main determinants of the slope are the kinetics of the electrocatalysis and the Ohmic loss.[13] The low Tafel slope suggests that the Ni-based OER catalysts have good activity and hole conducting layers allowing for efficient transportation without resistant loss.[13,32] The catalytic performance of the metal oxides (NiO_x, $NiRuO_x$, and sol−gel NiO_x) outperforms that of metal (Ni) because, presumably, better hole transfer can be obtained with the metal oxides due to the higher work function than the metals.[33] NiO_x, $NiRuO_x$, and sol−gel NiO_x showed comparable catalytic performance. The addition of Ru lowers the overpotential. A detailed discussion of the Ru and NiO_x composite is provided in ref 28. The overpotential required by ITO coated with sol−gel NiO_x can be as low as 0.346 V to achieve a current density of 1 mA/cm^2, which is close to the previously reported overpotential using a thick noble metal oxide[34−36] or an expensive catalyst fabrication method.[4]

DOI: 10.1021/nl5041463
Nano Lett. XXXX, XXX, XXX−XXX

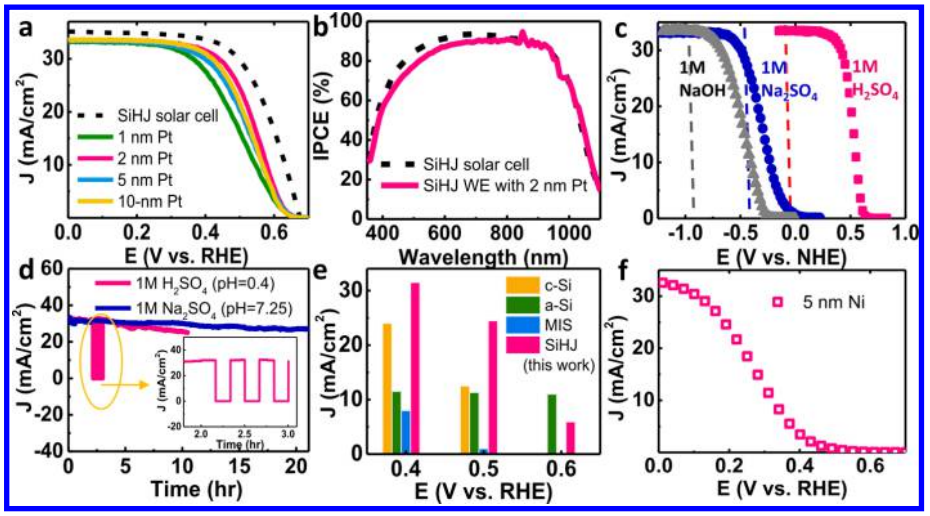

Figure 3. (a) $J-E$ curves of the SiHJ photocathodes with different thicknesses of Pt used as HER catalysts in a 1 M H_2SO_4 electrolyte under simulated AM 1.5G illumination. (b) IPCE measurement of the SiHJ photocathodes with 2 nm Pt used as the HER catalyst in a 1 M H_2SO_4 electrolyte under simulated AM 1.5G illumination. The integrated values of J_{H^+/H_2} is 33.43 mA/cm^2. (c) $J-E$ curves of the SiHJ photocathodes with 2 nm Pt used as the HER catalyst for acidic (pink symbol), neutral (blue symbol), and basic (gray symbol) electrolytes under simulated AM 1.5G illumination. Dashed vertical lines represent the thermodynamic redox potential for water reduction in the corresponding electrolyte. (d) Stability test results performed on a SiHJ photocathode sample with an area of 0.83 cm^2 in both acidic and neutral electrolytes. The inset in Figure 3d shows the stability test results with 1 h switching off /on of the light illumination. (e) Comparison of the photocurrent for various Si-based photocathodes reported in the literature and the current study at applied biases of 0.4, 0.5, and 0.6 V vs RHE. The data for the *c*-Si substrate, *a*-Si, and MIS photocathodes are taken from literature reports.[11,12,43] (f) $J-E$ curves of the SiHJ photocathode with cost-effective Ni used as the HER catalyst in a 1 M H_2SO_4 electrolyte under simulated AM 1.5G illumination.

The overpotentials and Tafel slopes measured under light illumination embody the performance of each component in the entire photoanode, including the SiHJ cell and the catalyst (specifically, the V_{OC}, J_{SC}, and FF of the solar cell, and transmittance and catalytic activity of the catalysts). Compare this with the overpotentials in the dark measurement, where the photovoltage was calculated to be 637 mV (dark ≈ +0.346 V, light ≈ −0.291 V for the sol−gel NiO_x catalyst). The increase in the Tafel slope under illumination mainly arises from the transmittance of the OER catalysts. For example, the low transmittance of $NiRuO_x$ leads the Tafel slope of $NiRuO_x$ to increase from 38.9 to 90 mV/decade, resulting in a low J_{H_2O/O_2} and SOCE. The Tafel slope of highly transparent sol−gel NiO_x still maintains a low value. The high transmittance, OER activity and cost- and time-effective synthesis of sol−gel NiO_x make it become one of the most promising OER catalyst candidates for photoanodes.[29]

SiHJ Photocathodes. PEC cells with Pt as a hydrogen-evolution-reaction (HER) catalyst on the back side of the SiHJ cells serve as photocathodes for hydrogen generation. Many researchers have sought to minimize recombination before the photogenerated free carriers participate in the water redox reaction by designing the PV and redox reaction to occur on the same side. This will facilitate the immediate transport of photocarriers to the electrolyte, to participate in the redox reaction. However, with this method, there is a partial sacrifice of the photocurrent due to optical attenuation by overlaying catalysts. Most of the HER catalysts (e.g., pure metal or metal alloys) will block the incident light if deposited directly on the surface of the light-receiving side.[1] It would be more effective to separate the PV from the water redox reaction, particularly for an integrated spontaneous solar water splitting cell (Figure 1e).[12,14] The key point to making a successful design for separating the PV and the water redox reaction is to achieve a low recombination rate of WE, avoiding photogenerated carrier recombination loss during the period of transport throughout the whole device (e.g., see the photogenerated electrons in Figure 1e). With our SiHJ PEC system, because of the good passivation by *a*-Si:H and high quality of n-type c-Si compared to the p-type c-Si devices, we achieve a long carrier lifetime and diffusion length of electrons. The photogenerated electrons can be efficiently transported throughout the whole SiHJ cell to participate in the redox reaction, neglecting the carrier recombination loss. The high performance is illustrated by the experimental results.

SHCE. Figure 3a shows linear voltammograms (LV) of the SiHJ photocathodes coated with different thicknesses of Pt measured under simulated AM 1.5G illumination. The SHCE is calculated as follows

$$\mathrm{SHCE} = \frac{|V_{OS}' - E^{0\prime}|J_{H^+/H_2}FF}{I_{ph}} \quad (2)$$

where J_{H^+/H_2} is the current density at $E^{0\prime}$. The characteristics of the photocathode are summarized in Table 3. The $J-E$ curves of the SiHJ photocathodes match those of the SiHJ cells well,

Table 3. Characteristics of SiHJ Photocathodes with Different Thicknesses of Pt Used as HER Catalysts in a 1 M H_2SO_4 Electrolyte under simulated AM 1.5G Illumination; the Onset Potential Was Measured at 1 mA/cm^2

	J_{H^+/H_2} (mA/cm^2)	$V_{OS}' - E^{0\prime}$ (V)	FF (%)	SHCE (%)
SiHJ solar cell	35.41	0.670	63.0	14.93
1 nm Pt	33.39	0.632	52.5	11.08
2 nm Pt	33.49	0.640	61.9	13.26
5 nm Pt	33.49	0.639	56.7	12.13
10 nm Pt	33.56	0.639	59.8	12.82

DOI: 10.1021/nl5041463
Nano Lett. XXXX, XXX, XXX−XXX

demonstrating that nearly all of the photovoltage generated by the SiHJ cells is delivered to the catalyst layer to drive the light-induced water reduction. The SiHJ photocathode with 2 nm thick Pt exhibits a $V_{OS}' - E^{0\prime}$ of 0.640 V, which is the highest value for c-Si photocathodes. For representative progress for Si-based photocathodes please see the comparison in Table S2 in Supporting Information. In addition, the J_{H^+/H_2} of the SiHJ photocathode with 2 nm thick Pt could be as high as 33.49 mA/cm^2. Very rapid bubble production of hydrogen gas was observed (see the Movie S1 in Supporting Information). There were two reasons for the high J_{H^+/H_2} achieved by the SiHJ photocathodes: (i) the light absorption in the WE was enhanced by the design where the PV and the water redox reaction were separated combined with light-trapping micropyramidal structures; (ii) the loss of photocarriers during transport throughout the whole device was decreased leaving more to participate in the water reduction process. Although it can be seen that some groups proposed a wire structured photocathode in order to increase the light absorption and catalyst loading, there was no significant improvement in their J_{H^+/H_2} and efficiency, which sometimes became even worse due to the poor surface passivation. Clearly, to make structures with enhanced performance, not only the light-harvesting ability but also the passivation problem have to be seriously considered. Note that hierarchical structures are promising candidates satisfying both requirements, with related applications now under investigation.[25,37] Finally, the high J_{H^+/H_2} and $V_{OS}'-E^{0\prime}$ of our SiHJ photocathodes with the pyramidal structure lead to a world-record high efficiency of 13.26% among all kinds of Si-based photocathodes.

Because the same amount of incident light enters the SiHJ PEC cells (the Pt catalyst was coated on the back sides of the cells), the J_{SC} and V_{OC} of the SiHJ photocathodes are independent of the Pt thickness. The major difference in the photocathodic behavior is the *FF*, i.e., the catalytic ability. The catalytic activity of Pt reaches its highest value and then decreases slightly with an increase in thickness of the Pt, which is consistent with other researchers' results.[38−40] For a small amount of Pt (1 nm thick Pt), the low catalytic ability might arise from insufficient catalyst loading and the noncrystalline nature of the material.[39] A large fraction of Pt atoms are on the surface. The surface interaction between the Pt atoms and ITO layers restricts the Pt crystallization. With the increase in Pt loading, the Pt atoms assemble in a more spherical fashion in order to minimize the surface energy, which is of benefit to Pt crystallization and carrier transport. Further increasing the amount of Pt leads to a slight decrease in the slope of the photocathodic *J*−*E* curve perhaps due to the formation of grain boundaries arising from the assembly of Pt nanoparticles[39] and lowering the surface to volume ratio (i.e., limited surface reaction sites), leading to a higher charge transfer resistance. The charge transfer resistance is investigated by electrochemical impedance spectroscopic (EIS) analysis (see Figure S7 in Supporting Information). The charge transfer resistance obtained from EIS can help to determine the active surface area and catalytic activity. The 2 nm thick Pt shows the lowest charge transfer resistance, demonstrating the highest catalytic ability.

Incident-Photon-Conversion Efficiency (IPCE). The IPCE was measured as a function of the wavelength for the SiHJ photocathode with 2 nm thick Pt at 0 V vs RHE (Figure 3b). The spot size (A_{ph} = 0.1 mm × 0.2 mm) of the monochromatic light on the sample surface was much smaller than the sample size. This was considered in the IPCE calculation. The photocurrent was calculated using the equation below: $j_{ph} = (I_{ph} - I_d)/A_{ph}$, where I_d is the dark current and I_{ph} is the current measured under light illumination; and A_{ph} is the light spot size.

$$\mathrm{IPCE} = \frac{1240 J_{ph}}{\lambda \frac{J_{ph}}{R_\lambda}} = \eta_{ext} \frac{J_{ph}}{J_{phD}} \tag{3}$$

where λ is the wavelength of incident light; J_{ph} is the measured photocurrent; J_{phD} is the photocurrent from the Si photodetector; R_λ is the responsitivity of the Si photodetector provided by the supplier; and η_{ext} is the external quantum efficiency of the Si photodetector. The IPCE of the SiHJ PEC cells matches the EQE of the SiHJ cells well. The IPCE rises quickly and reaches over 70% in the visible light region from 450 to 1000 nm with the highest value of 94% at 850 nm. The high IPCE over the broad-band wavelength range indicates the broad-band light absorption and efficient carrier transport in the SiHJ cells and between the SiHJ cell/ITO/Pt electrodes.

Working pH Range and Stability. In order to demonstrate that the SiHJ photocathode can efficiently work over a range of pH values, water reduction by the SiHJ photocathode with 2 nm thick Pt was measured under simulated AM 1.5G illumination in acidic (1 M H_2SO_4), neutral (1 M PBS buffered Na_2SO_4), and basic (1 M NaOH) electrolyte (Figure 3c). The characteristics of the photocathode are summarized in Table 4. Because of the buried junctions of the SiHJ PEC cells, the photovoltage of the solar-driven hydrogen evolution is not dependent on the pH of the electrolyte.[41] The photovoltage can be further confirmed by comparing the V_{OS} of the 2 nm Pt-coated SiHJ photocathode under illumination with the V_{OS} of the 2 nm Pt-coated ITO film in the dark in the 1 M Na_2SO_4 and 1 M NaOH electrolyte, respectively (see Figure S8 in Supporting Information). In addition to the performance tests carried out in different pH electrolytes, we also evaluated the lifetime of the SiHJ photocathodes in different pH electrolytes. Figure 3d shows the results of stability tests performed on a SiHJ photocathode sample with an area of 0.83 cm^2 in both the 1 M acidic electrolyte (pH = 0.4) at −0.0236 V vs NHE (0 V vs RHE) and 1 M neutral electrolyte (pH = 7.25) at −0.764 V vs NHE (0.336 V vs RHE, where the J_{SA} occurred). The stability of the SiHJ photocathode was tested for up to 10 h of operation in a 1 M acidic electrolyte. The inset to Figure 3d shows the results of stability test for 1 h switching off/on the light illumination. The current density returns back to the original value every time it is switched, revealing the good photoactivity of the SiHJ photocathode after the 3 h stability test. After 10 h of operation, the current density showed a decay of 8.37 mA/cm^2, which could be attributed to the decrease in resistivity of ITO

Table 4. Characteristics of SiHJ Photocathodes with 2 nm Pt Used as the HER Catalyst in Acidic, Neutral, and Basic Electrolytes under simulated AM 1.5G Illumination; the Onset Potential Was Measured at 1 mA/cm^2

	J_{H^+/H_2} (mA/cm^2)	$V_{OS}' - E^{0\prime}$ (V)	*FF* (%)	SHCE (%)
1 M H_2SO_4	33.49	0.640	61.9	13.26
1 M Na_2SO_4	26.51	0.407	19.6	2.03
l M NaOH	32.89	0.472	36.4	5.66

DOI: 10.1021/nl5041463
Nano Lett. XXXX, XXX, XXX−XXX

due to reduction under reductive conduction and then the loss of Pt due to unstable ITO support.[42] Operation in a neutral electrolyte showed longer stability (with a 6.38 mA/cm^2 decay after 20 h of operation) than operation in an acidic electrolyte. Figure S9 in Supporting Information shows the stability of SiHJ solar cell. The photocurrent is very stable after 20 h of operation, demonstrating that the light-induced degradation in *a*-Si can be negligible due to the usage of ultrathin *a*-Si:H.[18] Therefore, the decrease in current density of SiHJ photocathodes is mainly from electrical loss of ITO and less amount of Pt.

Comparison of Si-Based Photocathodes. The high performance of the SiHJ photocathode was highlighted by comparison with several quintessential Si-based photocathodes, including homojunction c-Si,[12] *a*-Si,[11] and metal−insulator−semiconductor (MIS) photocathodes.[43] The SiHJ photocathode exhibited a significantly greater current density compared to any other previously reported for Si photocathodes. Almost no current density was generated at 0.6 V vs RHE for the homojunction c-Si and MIS photocathodes. To enable water splitting without an external voltage bias, Si-based photoelectrodes need to gain additional energy through the multijunction design.[4] For a two-component illumination design, a Si photocathode can be integrated with a photoanode. The overall water splitting efficiency (i.e., solar-to-hydrogen (STH) production efficiency, η_{STH}) of the photoelectrolysis system is estimated by overlapping the individual $J-V$ curve obtained for each photocathode and photoanode and can be calculated using eq 4:[1,44]

$$\eta_{STH} = \frac{J_{op}(1.23V)}{I_{ph}} \quad (4)$$

where J_{OP} is the maximum operating current density for the integrated PEC system, which is the current density at the intersection of the two $J-V$ curves. In an integrated PEC system for achieving current matching, the final J_{OP} and η_{STH} of a serial combination of photoelectrodes is limited by the photoelectrode with the smallest photocurrent. The high photocurrent of our SiHJ photoelectrodes makes them a good candidate for the bottom cell in a two-component illumination design for obtaining high-efficiency water splitting without an external voltage bias.

Outlook for SiHJ Photoelectrodes. Finally, we replaced the Pt catalyst with the cost-effective Ni (Figure 3f). The catalytic performance of Ni was optimized as shown in Figure S10 in Supporting Information. The photocathode characteristics are summarized in Table 5. The SiHJ photocathode with

Table 5. Characteristics of SiHJ Photocathodes Coated with Cost Effective Ni as the HER catalyst in a 1M H_2SO_4 Electrolyte under Simulated AM 1.5G Illumination; the Onset Potential Was Measured at 1 mA/cm^2

	J_{H^+/H_2} (mA/cm^2)	$V_{OS}' - E^{0\prime}$ (V)	*FF* (%)	SHCE (%)
5 nm Ni	32.79	0.475	30.97	4.84

Ni showed a high current density (>30 mA/cm^2) at 0 V vs RHE under 1 sun AM 1.5G illumination. This result demonstrates the potential of SiHJ photocathodes for cost-effective applications. It is worth noting that these SiHJ photoelectrodes can still be further optimized by including light-trapping structures for enhancing light absorption and surface reactive sites, grid contact electrodes for improving carrier collection, and protective layers for prolonged stability. When sunlight passes through a liquid, the light is easily scattered (diffused). Accordingly, omnidirectional performance of the photoelectrode is desired. Hierarchical structures have been shown to exhibit favorable omnidirectional broad-band light-trapping ability without causing serious recombination loss.[25,37,45] Improving carrier transport by the use of grid contact electrodes can increase the *FF*, which could potentially lead to a steep increase in the J_{OP} of an integrated PEC system.[41] By optimizing these conditions, it should be possible to achieve an SHCE for a SiHJ photocathode of higher than 15%. The SiHJ photoelectrochemical cell is an attractive candidate for practical solar fuel production due to its scalability and low cost.

■ ASSOCIATED CONTENT

Supporting Information

Experimental methods; additional figures and tables; video of rapid hydrogen evolution by a SiHJ photocathode sample. This material is available free of charge via the Internet at http://pubs.acs.org.

■ AUTHOR INFORMATION

Corresponding Authors

*E-mail: jrhau.he@kaust.edu.sa.

*E-mail: d.w.wang@ieee.org.

Author Contributions

The project was conceived by H.P.W., K.S., J.H.H., and D.W.; H.P.W. performed the experiments with help from S.Y.N., A.K., M.L.T., and M.Y.H.; they also analyzed the data and wrote the manuscript with K.S., J.H.H. and D.W.

Notes

The authors declare no competing financial interest.

■ ACKNOWLEDGMENTS

D.W. acknowledges the financial support for this work by the National Science Foundation (CBET1236155). D.W. thanks Drs. R. Rao and B. Fruhberger from Qualcomm Institute of UCSD for their unconditional support. The authors thank the staff of UCSD Nano3 facilities for their timely and professional support. The authors acknowledge KAUST, National Science Council of Taiwan and National Taiwan University.

■ REFERENCES

(1) Walter, M. G.; Warren, E. L.; McKone, J. R.; Boettcher, S. W.; Mi, Q.; Santori, E. A.; Lewis, N. S. *Chem. Rev.* **2010**, *110*, 6446−6473.

(2) Hu, S.; Xiang, C.; Haussener, S.; Berger, A. D.; Lewis, N. S. *Energy Environ. Sci.* **2013**, *6*, 2984−2993.

(3) McKone, J. R.; Lewis, N. S.; Gray, H. B. *Chem. Mater.* **2014**, *26*, 407−414.

(4) Sun, K.; Shen, S.; Liang, Y.; Burrows, P. E.; Mao, S. S.; Wang, D. *Chem. Rev.* **2014**, *114*, 8662−8719.

(5) Chen, Y. W.; Prange, J. D.; Dühnen, S.; Park, Y.; Gunji, M.; Chidsey, C. E. D.; McIntyre, P. C. *Nat. Mater.* **2011**, *10*, 539−544.

(6) Seger, B.; Pedersen, T.; Laursen, A. B.; Vesborg, P. C. K.; Hansen, O.; Chorkendorff, I. *J. Am. Chem. Soc.* **2013**, *135*, 1057−1064.

(7) Kenney, M. J.; Gong, M.; Li, Y.; Wu, J. Z.; Feng, J.; Lanza, M.; Dai, H. *Science* **2013**, *342*, 836−840.

(8) Seger, B.; Tilley, D. S.; Pedersen, T.; Vesborg, P. C. K.; Hansen, O.; Gratzel, M.; Chorkendorff, I. *RSC Adv.* **2013**, *3*, 25902−25907.

(9) Choi, M. J.; Jung, J.-Y.; Park, M.-J.; Song, J.-W.; Lee, J.-H.; Bang, J. H. *J. Mater. Chem. A* **2014**, *2*, 2928−2933.

DOI: 10.1021/nl5041463
Nano Lett. XXXX, XXX, XXX−XXX

(10) Hu, S.; Shaner, M. R.; Beardslee1, J. A.; Lichterman, M.; Brunschwig, B. S.; Lewis, N. S. *Science* **2014**, *344*, 1005−1009.
(11) Lin, Y.; Battaglia, C.; Boccard, M.; Hettick, M.; Yu, Z.; Ballif, C.; Ager, J. W.; Javey, A. *Nano Lett.* **2013**, *13*, 5615−5618.
(12) Boettcher, S. W.; Warren, E. L.; Putnam, M. C.; Santori, E. A.; Turner-Evans, D.; Kelzenberg, M. D.; Walter, M. G.; McKone, J. R.; Brunschwig, B. S.; Atwater, H. A.; Lewis, N. S. *J. Am. Chem. Soc.* **2011**, *133*, 1216−1219.
(13) Cox, C. R.; Winkler, M. T.; Pijpers, J. J. H.; Buonassisi, T.; Nocera, D. G. *Energy Environ. Sci.* **2013**, *6*, 532−538.
(14) Pijpers, J. J. H.; Winkler, M. T.; Surendranath, Y.; Buonassisi, T.; Nocera, D. G. *Proc. Natl. Acad. Sci. U.S.A.* **2011**, *108*, 10056−10061.
(15) Yang, J.; Walczak, K.; Anzenberg, E.; Toma, F. M.; Yuan, G.; Beeman, J.; Schwartzberg, A.; Lin, Y.; Hettick, M.; Javey, A.; Ager, J. W.; Yano, J.; Frei, H.; Sharp, I. D. *J. Am. Chem. Soc.* **2014**, *136*, 6191−6194.
(16) Nozik, A. J. *Appl. Phys. Lett.* **1976**, *29*, 150−153.
(17) Terlinden, N. M.; Dingemans, G.; van de Sanden, M. C. M.; Kessels, W. M. M. *Appl. Phys. Lett.* **2010**, *96*, 112101−112101−3.
(18) Sawada, T.; Terada, N.; Tsuge, S.; Baba, T.; Takahama, T.; Wakisaka, K.; Tsuda, S.; Nakano, S. In *Proceedings of 24th IEEE Photovoltaics Specialists Conference*, Waikoloa, Hawaii, 5−9 December, 1994; Vol. 2, pp 1219−1226.
(19) Olibet, S. *Phys. Status Solidi A* **2010**, *207*, 651−656.
(20) Yablonovitch, E.; Gmitter, T.; Swanson, R. M.; Kwark, Y. H. *Appl. Phys. Lett.* **1985**, *47*, 1211−1213.
(21) Wang, H. P.; Lin, T. Y.; Tsai, M. L.; Tu, W. C.; Huang, M. Y.; Liu, C. W.; Chueh, Y. L.; He, J. H. *ACS Nano* **2014**, *8*, 2959−2969.
(22) Panasonic Corp. Panasonic HIT Solar Cell Achieves World's Highest Energy Conversion Efficiency of 25.6% at Research Level, 2014. http://panasonic.co.jp/corp/news/official.data/data.dir/2014/04/en140410-4/en140410-4.html.
(23) Hwang, Y. J.; Boukai, A.; Yang, P. *Nano Lett.* **2008**, *9*, 410−415.
(24) Oh, I.; Kye, J.; Hwang, S. *Nano Lett.* **2011**, *12*, 298−302.
(25) Wang, H. P.; Lin, T. Y.; Hsu, C. W.; Tsai, M. L.; Huang, C. H.; Wei, W. R.; Huang, M. Y.; Chien, Y. J.; Yang, P. C.; Liu, C. W.; Chou, L. J.; He, J. H. *ACS Nano* **2013**, *7*, 9325−9335.
(26) Smith, R. D. L.; Prévot, M. S.; Fagan, R. D.; Zhang, Z.; Sedach, P. A.; Siu, M. K. J.; Trudel, S.; Berlinguette, C. P. *Science* **2013**, *340*, 60−63.
(27) Sun, K.; Park, N.; Sun, Z.; Zhou, J.; Wang, J.; Pang, X.; Shen, S.; Noh, S. Y.; Jing, Y.; Jin, S.; Yu, P. K. L.; Wang, D. *Energy Environ. Sci.* **2012**, *5*, 7872−7877.
(28) Sun, K.; Pang, X.; Shen, S.; Qian, X.; Cheung, J. S.; Wang, D. *Nano Lett.* **2013**, *13*, 2064−2072.
(29) Sun, K.; Shen, S.; Cheung, J. S.; Pang, X.; Park, N.; Zhou, J.; Hu, Y.; Sun, Z.; Noh, S. Y.; Riley, C. T.; Yu, P. K. L.; Jin, S.; Wang, D. *Phys. Chem. Chem. Phys.* **2014**, *16*, 4612−4625.
(30) McCrory, C. C. L.; Jung, S.; Peters, J. C.; Jaramillo, T. F. *J. Am. Chem. Soc.* **2013**, *135*, 16977−16987.
(31) Chen, Z.; Jaramillo, T. F.; Deutsch, T. G.; Kleiman-Shwarsctein, A.; Forman, A. J.; Gaillard, N.; Garland, R.; Takanabe, K.; Heske, C.; Sunkara, M.; McFarland, E. W.; Domen, K.; Miller, E. L.; Turner, J. A.; Dinh, H. N. *J. Mater. Res.* **2010**, *25*, 3−16.
(32) Corrigan, D. A. *J. Electrochem. Soc.* **1987**, *134*, 377−384.
(33) Greiner, M. T.; Chai, L.; Helander, M. G.; Tang, W.-M.; Lu, Z.-H. *Adv. Funct. Mater.* **2012**, *22*, 4557−4568.
(34) Nakagawa, T.; Bjorge, N. S.; Murray, R. W. *J. Am. Chem. Soc.* **2009**, *131*, 15578−15579.
(35) Yagi, M.; Tomita, E.; Sakita, S.; Kuwabara, T.; Nagai, K. *J. Phys. Chem. B* **2005**, *109*, 21489−21491.
(36) Ouattara, L.; Diaco, T.; Duo, I.; Panizza, M.; Foti, G.; Comninellis, C. *J. Electrochem. Soc.* **2003**, *150*, D41−D45.
(37) Wei, W. R.; Tsai, M. L.; Ho, S. T.; Tai, S. H.; Ho, C. R.; Tsai, S. H.; Liu, C. W.; Chung, R. J.; He, J. H. *Nano Lett.* **2013**, *13*, 3658−3663.
(38) Peng, K.-Q.; Wang, X.; Wu, X.-L.; Lee, S.-T. *Nano Lett.* **2009**, *9*, 3704−3709.
(39) Somik, M.; Balavinayagam, R.; Lauren, G.; Steven, H.; Gary, A. B.; Phil, F.; Shramik, S.; Shubhra, G. *Nanotechnology* **2012**, *23*, 485405.
(40) Lombardi, I.; Marchionna, S.; Zangari, G.; Pizzini, S. *Langmuir* **2007**, *23*, 12413−12420.
(41) Warren, E. L.; Boettcher, S. W.; Walter, M. G.; Atwater, H. A.; Lewis, N. S. *J. Phys. Chem. C* **2010**, *115*, 594−598.
(42) Folcher, G.; Cachet, H.; Froment, M.; Bruneaux, J. *Thin Solid Films* **1997**, *301*, 242−248.
(43) Esposito, D. V.; Levin, I.; Moffat, T. P.; Talin, A. A. *Nat. Mater.* **2013**, *12*, 562−568.
(44) Weber, M. F.; Dignam, M. J. *J. Electrochem. Soc.* **1984**, *131*, 1258−1265.
(45) Wang, H. P.; Lien, D. H.; Tsai, M. L.; Lin, C. A.; Chang, H. C.; Lai, K. Y.; He, J. H. *J. Mater. Chem. C* **2014**, *2*, 3144−3171.

DOI: 10.1021/nl5041463
Nano Lett. XXXX, XXX, XXX−XXX